# Molecular dynamics study of dislocation nucleation from a crack tip

Berk Hess,[1] Barend J. Thijsse,[2] and Erik Van der Giessen[1]
[1]*Department of Applied Physics, University of Groningen, Nijenborgh 4,9747 AG, Groningen, The Netherlands*
[2]*Laboratory of Materials Science and Engineering, Delft University of Technology, Rotterdamseweg 137, 2628 AL, Delft, The Netherlands*
(Received 7 July 2004; revised manuscript received 12 October 2004; published 23 February 2005)

We have performed a systematic molecular dynamics study of the competition between crack growth and dislocation emission from a crack tip. Two types of boundary conditions are adopted: either planar extension or boundary displacements according to the anisotropic mode-I asymptotic continuum solution. The effects of temperature, loading rate, crystal orientation, sharpness of the crack tip, atomic potential, and system size are investigated. Depending on the crystal orientation, dislocation nucleation can be driven either by the strain or by concerted fluctuations at the crack tip. In the latter case, crystal orientation and temperature have the largest influence on the process of dislocation nucleation.

DOI: 10.1103/PhysRevB.71.054111 PACS number(s): 62.20.Mk, 61.72.Lk, 31.15.Qg

## I. INTRODUCTION

The brittle vs ductile response of crystalline materials is mainly controlled by the competition between crack growth and the mobility of dislocations near the crack tip. In materials that have a low initial dislocation density, the emission of a dislocation from the crack tip is a critical event. The modeling of dislocation emission vs crack propagation was initiated with a two-dimensional analysis (2D) analysis based on the Peierls concept by Rice,[1,2] and later extended to 3D.[3,4] Xu *et al.*[5] have determined that for $\alpha$-Fe and Si the activation energy to emit dislocations in any direction from a straight crack front is higher than that for crack propagation. They propose a ledge configuration to allow for dislocation emission.[6] The advantages of this type of modeling are that it gives direct insight into competing forces and produces activation energies for dislocation nucleation. However, it is questionable if a continuum approach is valid for a system where the saddle-point structure is of the size of only a few atoms. To avoid this problem one has to revert to atomistic simulations.

Atomistic simulations of materials containing a mode-I crack can be carried out with two types of boundary conditions: planar extension or coupled to a continuum solution. Due to the high computational demands on atomic systems, their size is limited to about 1 $\mu$m$^3$. As specimens used in experiments are usually much larger, the atomistically described part of the system must be restricted to a small region around the crack tip. For this reason, the planar-extension boundary condition corresponds to a situation where the material outside the simulated sample does not feel the response of the sample. This is only possible when a shock wave passes through the material. When loading is sufficiently slow, the boundaries of the atomic part can be coupled to the well-known continuum quasistatic solution (asymptotically) close to the crack tip. This ensures full communication between the crack tip region and the remote material. Shock-wave simulations have the advantage that dislocation nucleation and motion happen on a very short time scale, which makes large systems feasible; see, for instance, Zhou *et al.*[7] who have used Morse and embedded atom model (EAM) potentials on systems with many millions of atoms at nearly zero temperature. A very large system, one billion atoms, has been simulated by Abraham *et al.*,[8] but starting from a block with two small cuts at 0 K, which has been prestrained in mode-I loading (such a setup is impossible to achieve experimentally). The first atomistic calculation coupled to a continuum was performed by Gehlen *et al.*[9,10] in 2D using $K_I$-continuum boundary conditions on the atomic region. Quasi-3D calculations (using a minimal periodic spacing) with a finite element grid in between the continuum boundary and the atomistic part have been performed by Gumbsch,[11] while Miller *et al.*[12] have used a quasicontinuum approach. All these studies are quasistatic, involving a number of static energy minimizations at different load levels.

As the above summary shows, most atomistic studies have been performed quasistatically or at near-zero temperature. However, temperature is an essential factor, as is evident from the existence of a brittle-ductile transition temperature. Temperature influences the response of the system in two ways. The stiffness of most materials decreases with increasing temperature. But a more important effect is that a higher thermal energy makes it easier to overcome energy barriers. This will facilitate both crack propagation and dislocation nucleation. At finite temperatures the loading rate also becomes important. Beside these, crack propagation and dislocation nucleation are determined by geometric features, including crystal orientation, crack height, crack front profile, and the smoothness of the crack surface.

In this paper we present a systematic molecular dynamics (MD) study of the effect of temperature and loading rate on the emission of dislocations from a crack tip for three crystal orientations, with a flat crack surface and a sharp or slightly blunt crack tip with a straight crack front. We use a Lennard-Jones (LJ) potential, a similar Morse potential and an EAM potential for nickel. Although the LJ and Morse potentials do not model metals as well as the EAM potential, we do not expect the general trends to be vastly different. An important indicator of this is that the generalized stacking fault energy—one of the most important properties for dislocation nucleation—is the same for the LJ potential and more advanced potentials for nickel and copper.[13] We compare the

 

results of planar-extension boundary conditions and boundary conditions based on the $K_I$-continuum solution.

## II. METHODS

The first of the two pair potentials we consider is the LJ potential

$$V_p(r) = 4\epsilon\left[\left(\frac{\sigma}{r}\right)^{12} - \left(\frac{\sigma}{r}\right)^{6}\right],$$

where $r$ is the distance between two particles, $\epsilon$ is the depth of the energy minimum, and $\sigma$ is the distance at which the potential is zero. The second is a Morse potential

$$V_p(r) = \epsilon\left\{\exp\left[-12\left(\frac{r}{r_m}-1\right)\right] - 2\exp\left[-6\left(\frac{r}{r_m}-1\right)\right]\right\}$$

where $r_m$ is the position of the minimum. When $\sigma = 2^{-1/6} r_m$ the position and depth of the minima of both potentials are equal, and so is the second derivative at the minimum. The main difference between the two potentials is that the LJ potential is longer ranged than the Morse potential.

For efficiency reasons we use a cutoff for the pair interactions: all interactions beyond a distance of $r_c$ are neglected. An abrupt cutoff of the interactions introduces artifacts as pairs move in and out of the cutoff distance. This introduces fluctuations which very slowly induce phonon modes that can lead to dislocation nucleation. Under the conditions as described later on, but with a plain cutoff, we have observed the growth of phonon modes leading to dislocation nucleation on time scales ranging from 10 ps to as long as 3000 ps. To avoid these artifacts we apply a switch function in combination with a shift by replacing the pair potential $V_p$ by

$$V_s(r) = \begin{cases} V_p(r) - C, & r \leqslant r_s, \\ V_p(r) - A(r-r_s)^3 - B(r-r_s)^4 - C, & r_s < r < r_c, \\ 0, & r \geqslant r_c. \end{cases} \tag{1}$$

The constants $A$, $B$, and $C$ are chosen such that potential and its first and second derivatives are zero at $r_c$. Thus the forces are unaltered up to distance $r_s$. The shift $C$ is $0.006\epsilon$ and $0.001\epsilon$ for the LJ and Morse potentials respectively, with the cutoffs as listed in Table I. The shifted potential produces a smooth and accurate stress-strain curve. With an abrupt cutoff there are jumps in the stress when the increasing distance between atoms exceeds the cutoff. A switch function (without shift) may also smooth these jumps, but it will enlarge the forces near the cutoff, which also introduces irregularities in the stress-strain curve. All LJ and Morse simulations have been performed in reduced units with the GROMACS simulation software.[14,15]

The EAM potential has a density term as well as a pair term. The parameters were taken for nickel from Oh and Johnson.[16] To compare the results with the EAM potential, we have fitted the length scale using the lattice spacing and the energy scale using the elastic constants. The parameters for the LJ potential thus become $\sigma = 0.226$ nm, $\epsilon = 2.90 \times 10^{-20}$ J and for the Morse potential $r_m = 0.256$ nm, $\epsilon = 3.45 \times 10^{-20}$ J. All LJ and Morse simulations to be presented here have used a time step of 0.004 ps and a neighbor list that is updated every 20 integration steps. The neighbor list is built with a cutoff that is 0.011 nm larger than $r_c$, in order to ensure that no atom pairs outside the list will come within interaction range between updates. To keep the system at constant temperature it is coupled to a heat bath using a Berendsen thermostat[17] with a coupling time of 0.1 ps. On a single 2.6 GHz Pentium 4 processor, Morse and LJ systems of 96 000 atoms run at 13 000 and 19 000 steps (54 and 73 ps) per CPU hour, respectively. The times for the larger systems scale linearly with the number of atoms. For the EAM simulations the time step is 0.005 ps and the neighbor list is updated using a displacement criterion. On the same processor the system of 96 000 atoms runs at 2200 steps (i.e., 11 ps) per CPU hour.

TABLE I. The nearest neighbor distance $r_1$ and elastic moduli of fcc crystals with three different potentials at 0 and 300 K. The LJ and Morse potentials use the shift function (1), which switches the forces smoothly to zero between $r_s$ and $r_c$. The experimental values for nickel were taken from Alers *et al.* (Ref. 18).

| Potential | $r_c$ (nm) | $r_s$ (nm) | $T$ (K) | $r_1$ (nm) | $C_{11}$ | $C_{12}$ (GPa) | $C_{44}$ |
|---|---|---|---|---|---|---|---|
| LJ | 0.678 | 0.655 | 0 | 0.249 | 245 | 139 | 138 |
| LJ | 0.678 | 0.655 | 300 | 0.250 | 200 | 113 | 113 |
| Morse | 0.593 | 0.570 | 0 | 0.249 | 234 | 137 | 136 |
| Morse | 0.593 | 0.570 | 300 | 0.250 | 202 | 120 | 122 |
| EAM | 0.473 | | 0 | 0.249 | 232 | 150 | 128 |
| EAM | 0.473 | | 300 | 0.250 | 216 | 139 | 116 |
| Ni expt. | | | 300 | | 245 | 140 | 125 |

To determine the lattice spacing and the energy of perfect fcc crystals at zero pressure, we have performed simulations with Berendsen pressure coupling.[17] The results for the three potentials at 0 and 300 K are listed in Table I. The three elastic moduli of the fcc crystals are determined from simulations of uniform straining by 0.001 in the [100] and [110] directions. The moduli for the LJ crystal are 5% smaller than without a cutoff, while the cutoff effect for the Morse crystal is less than the accuracy of the simulations. These differences are negligible compared to the strong nonlinearity of the elastic response. All elastic constants are reduced by 50% at uniaxial strains in the range from 0.05 to 0.1, with the reduction being largest for the LJ potential.

## III. PLANAR-EXTENSION BOUNDARY CONDITIONS

With the planar-extension boundary conditions we aim to simulate a shock wave passing through a crack tip region in a monocrystal which is much larger than the simulated system in all three spatial directions. The wave front is chosen to be parallel to the crack plane. It travels with the speed of sound, which is 5.0 nm ps$^{-1}$, experimentally as well as for the three potentials.

First we describe the geometry of the system. We adopt the same orientation as Zhou *et al.*:[7] the crack is on the (100)

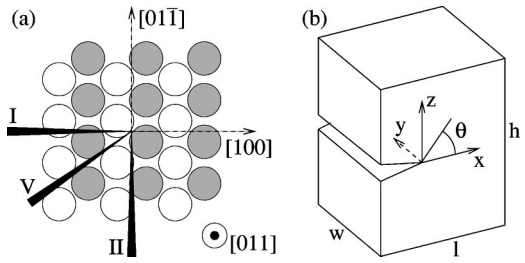


FIG. 1. (a) The three crystal orientations I, II, and V with respect to the crack. (b) The coordinate system and definition of the angle $\theta$ of the plane through the crack front, coinciding with the $y$ axis.

plane and the crack front is in the [011] direction. This corresponds to crystal orientation II in Fig. 1(a). The coordinate system at the crack tip is defined in Fig. 1(b). The crack length is a third of the size $\ell$ of the system in the $x$ direction. To mimic a large system the $y$ direction is made periodic. Atoms on the $z=\pm h/2$ plane boundaries are fixed in all three directions using harmonic springs. The spring constant is chosen such that the boundary atoms vibrate with the same frequency as in the bulk. The atoms on the $x=-\ell/3$ and $x=2\ell/3$ plane boundaries are fixed with springs in the $x$ and $y$ directions, but free in the $z$ direction, which allows the shock wave to pass through undistortedly. By contrast, free boundaries on these planes would allow them to move inward due to the high stresses and such a setup thus would simulate a specimen of only a few nanometers.

The size of the system limits the scales, both in time and in length, that can be simulated. When the shock wave has reached the crack it will reflect and travel back to the boundary. After this wave has reached the boundary, an artifact will move into the system. This holds for all four nonperiodic boundary planes. The periodic direction is less critical, as the shock wave produces a relatively uniform response in this direction. Considering this we choose the dimensions as $\ell \times w \times h = 100 \times 60 \times 160 = 960\,000$ atoms, which gives a size of $25 \times 15 \times 28$ nm$^3$. Because we want to start from an unstressed starting configuration, we need to remove one or more atomic planes to create a crack. We choose to remove four atomic planes, which ensures that the two crack faces will not attract each other. The crack tip was chosen somewhat rounded, since a rectangular crack tip is not very stable under loading due to the stress concentrations at the corners.

We performed simulations with the LJ potential at 21, 210, and 420 K and with the Morse potential at 25, 250, and 500 K. Each of the six systems was equilibrated using stochastic dynamics with a friction constant of 2.5 ps$^{-1}$. This ensures a proper potential and kinetic energy distribution. The friction also damps waves that are generated by the slight mismatch of the initially perfect crystal with the boundary conditions and with the free surface at the crack.

Subsequently, shock-wave simulations were performed by pulling the $z=h/2$ plane in the $+z$ direction with a constant velocity of 0.28 or 0.42 nm ps$^{-1}$ while fixing the $z=-h/2$ plane (at a higher velocity of 0.56 nm ps$^{-1}$ the stress is too high and the top layer of atoms dissociates from the rest of the system). The simulations were performed without temperature coupling; this is permitted since the energy drift within the simulation time of 8 ps is negligible. With the chosen pulling rates, a straight wave front propagates through the system. The initial block wave is smeared out over a length of 6 nm when it reaches the crack. As the shock wave passes through the crack, the crack tip is stretched to such an extent that locally the crystal structure is lost. In all simulations Shockley partial dislocations are then emitted on the $(11\bar{1})$ and $(1\bar{1}1)$ slip planes that pass through the crack tip. First, two dislocations are emitted in the two forward (i.e., positive $x$) directions. At an extension velocity of 0.42 nm ps$^{-1}$ backward dislocations are observed in all cases, except for the Morse potential at the highest temperature. At the lowest velocity only the systems with the LJ potential at the two lowest temperatures emit backward dislocations. As the strain increases, more Shockley partial dislocations are emitted on the same slip planes or on adjacent ones. Under the same conditions, more dislocations are observed with the LJ potential than with the Morse potential. After a time of 6.8 ps the reflected shock wave reaches the upper boundary, which limits the simulation time to a few picoseconds after this. Figure 2 shows the stress field at 7.0 ps for the simulation with the LJ potential at the lowest temperature with an extension velocity of 0.42 nm ps$^{-1}$.

## IV. CONTINUUM-SOLUTION BOUNDARY CONDITIONS

When no fast processes take place close to the crack tip and there are no crystal defects in its vicinity, the crack tip region can be treated as an elastic continuum. A static solution can be derived analytically, which can then be used as a boundary condition for the atomic simulation. Since a fcc crystal is a cubic material, an anisotropic continuum solution (Sih and Leibowitz[19]) is required, which for mode-I loading is given in the Appendix. As long as the atomic part responds linearly, the continuum solution can also be used quasistatically, i.e., with increasing load level $K_I$. At a certain stress level, the near-crack-tip region will exhibit a nonlinear response. This is not problematic as long as this region is small compared to the size of the atomic box so that the boundary is not affected by nonlinearity. Even when a dislocation has nucleated, this so-called small-scale yielding condition can be satisfied when it does not travel too close to the boundary.

In fcc metals the dominant slip systems are associated with {111} planes; therefore we place the crack front in a {111} plane along the [011] direction. We choose the three orientations for the crack plane that give the smoothest crack surfaces: $(01\bar{1})$, $(1\bar{1}1)$, and (100), which we call orientations I, V, and II, respectively (adopting the numbering suggested by Crone *et al.*[20]); see Fig. 1(a). Orientations V and II differ from orientation I by a 35.3° and 90° rotation about the $y$ axis, respectively. With the same crack front, along [011], one could choose any of the orientations in between I and II, but all of these except V have stepped crack surfaces. We will see later that with two of these three orientations one can cover the most relevant types of behavior with a ⟨011⟩ crack front.

In choosing the size there are several aspects that need to be considered. The size along the $y$ direction of the crack front should be larger than the width of a nucleating disloca-

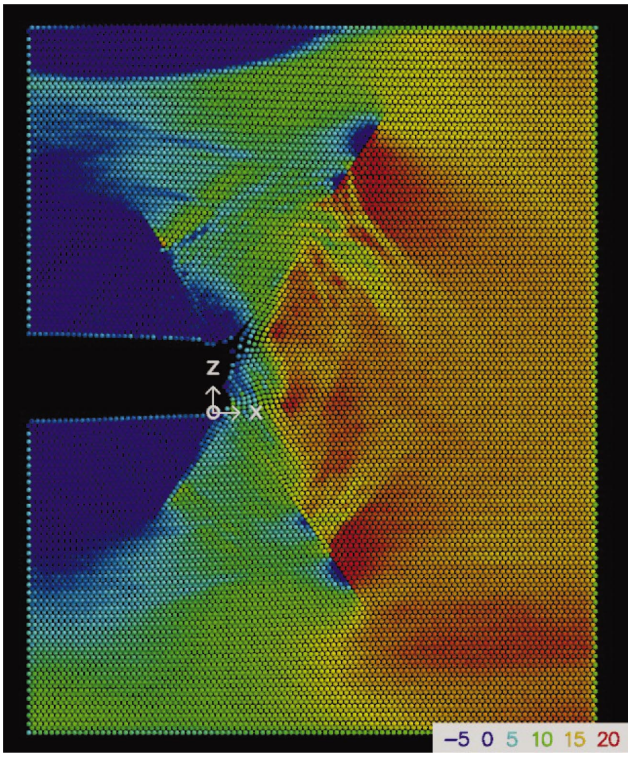


FIG. 2. (Color) The $\sigma_{zz}$ stress distribution (in GPa) in crystal orientation II at time 7.0 ps for the $1\times10^6$ atom, planar-extension simulation with LJ potential, at temperature 21 K with an extension velocity of 0.42 nm ps$^{-1}$. The strain between the top and bottom boundaries is roughly 10%. The origin of the coordinate system is at the original position of the crack tip in the unloaded starting configuration; the $y$ axis is along the crack front pointing into the picture; cf. Fig. 1(b). The coordinates and the stress have been averaged over the 60 atoms along the crack front direction. The atomic positions at the crack tip differ too much to give a meaningful average. Slip planes with dislocations can be seen above and below the center of the picture as sharp green/red demarcations and on the left as sharp blue/green demarcations. The blue region in the upper left-hand corner indicates the shock wave which has traveled to the crack and back and has just reflected off the top boundary.

tion. In the other two directions the boundary of the system should be far enough from the crack tip that small-scale yielding is satisfied. Increasing the system size increases the range, both in space and in time, over which events can be observed. We will show later that dislocation nucleation is associated with the correlated displacement of a row of 10 to 20 atoms. To avoid artifacts, we use a minimum size along the crack of 40 atoms. We choose one or two system sizes for each of the three orientations; all dimensions are listed in Table II. The load levels will be reported in dimensionless strain, $K_I/\sqrt{r_1\mu}$, where $r_1$ is the fcc nearest neighbor distance.

### A. Orientation I

First we tried an atomically sharp crack. Because the two crack surfaces attract each other at short range, we need to start from a sufficiently strained conformation. We transformed a perfect crystal using the continuum solution at various strain levels. These conformations were then energy minimized while the border atoms were fixed to the continuum solution using springs. At strain levels up to $K_I/\sqrt{r_1\mu}=0.47$ for the LJ potential and 0.43 for the Morse potential, where $\mu=C_{44}$, the [011] rows of atoms on the top and bottom crack surfaces closest to the crack tip attract each other and the crack closes over a length of several rows. These rows are relatively close due to the alternating $z$ positions of the rows on the $(01\bar{1})$ surface. At higher strain levels the crack does not close and a minimized conformation can be obtained. As a next equilibration step we performed stochastic dynamics at 20 K with a friction constant of 2.5 ps$^{-1}$, starting with zero velocities. Within a time span of a few picoseconds Shockley partial dislocations appear on one or both of the forward {111} slip planes at $\theta=\pm35.3°$. These partials are relatively easy to nucleate since the Burgers vector is in the $x$-$z$ plane; see Fig. 3. From these results we conclude that an atomically-sharp crack in this orientation is not stable.

Second we studied a blunt crack tip, which was obtained by removing four layers of atoms. Starting from perfect crystals at $K_I/\sqrt{r_1\mu}=0$ and 0.38 we equilibrated conformations for 4 ps for the LJ potential at 21 and 210 K, the Morse potential at 25 and 250 K, and the EAM potential at 300 K. From these conformations we ran MD simulations at four loading rates ranging from $\dot{K}_I/\sqrt{r_1\mu}=2.5\times10^{-2}$ to $1.0\times10^{-3}$ ps$^{-1}$. In all 22 simulations the first event is the nucleation of a Shockley partial at the crack tip with the Burgers vector pointing forward and upward (see Fig. 3). This happens at a load level of around 0.42 for all three potentials. The load levels are given in Table III, where we have defined the nucleation time as the time when three or more atoms have passed the transition point, which is halfway between

TABLE II. The system sizes used in the simulations with continuum-solution boundary conditions for the three different crystal orientations.

| | | No. of atom layers | | | Size (nm) | | | Crack length |
|---|---|---|---|---|---|---|---|---|
| Orientation | No. of atoms | $x$ | $y$ | $z$ | $x$ | $y$ | $z$ | (nm) |
| I | 96 000 | 60 | 40 | 40 | 10.6 | 10.0 | 10.0 | 3.7 |
| I | 256 000 | 64 | 80 | 50 | 11.3 | 20.0 | 12.5 | 3.9 |
| V | 96 000 | 40 | 40 | 60 | 8.7 | 10.0 | 12.8 | 2.9 |
| II | 96 000 | 40 | 40 | 60 | 10.0 | 10.0 | 10.6 | 3.5 |
| II | 320 000 | 50 | 80 | 80 | 12.5 | 20.0 | 14.1 | 4.1 |

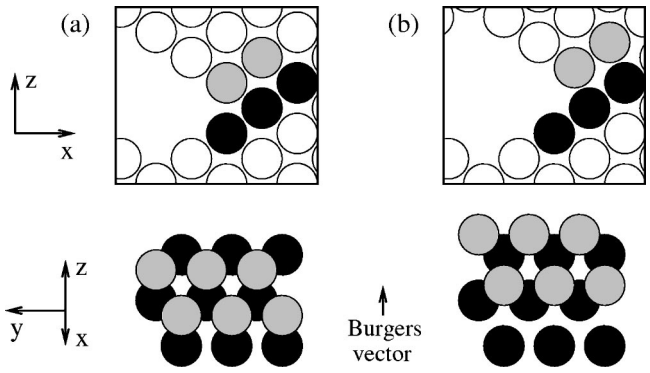


FIG. 3. Schematic drawing of the crack-tip region in orientation I before (a) and after (b) nucleation of a Shockley partial dislocation.

the original and the fully dislocated positions. The preference for the upward direction is caused by the asymmetry of the crack tip due to the removal of an even number of atomic planes. In most cases a row of roughly ten atoms crosses simultaneously, after which the dislocation bows out at a speed of, 2 nm ps$^{-1}$. This leads to a decrease in potential energy as well as in the stresses near the crack tip. The dislocation stops near the corner at the $x=2\ell/3$ and $z=h/2$ boundaries which causes a local stress concentration. Although at this point the boundary conditions have lost validity, the stress profiles near the crack tip have not changed drastically. The second dislocation is nucleated at a load level that is 0.06 higher than that of the first one. This dislocation behaves similarly to the first one, except that its slip plane and Burgers vector point downward instead of upward.

### B. Orientation V

Orientation V is an asymmetric orientation, because the crack plane does not coincide with a symmetry plane of the crystal. Since the crack is now on the $(1\bar{1}1)$ plane, there is only one {111} slip-plane orientation left that is parallel to the crack front: the $(11\bar{1})$ plane with $\theta=-70.5°$ in Fig. 1. As in orientation I, we minimized perfect crystals with an atomically sharp crack tip, starting from conformations that were prestrained using the continuum solution. At load levels up to $K_I/\sqrt{r_1}\mu=0.38$ for the LJ potential and 0.36 for the Morse potential the two crack faces attract each other and the crack closes. At higher strain levels a Shockley partial dislocation on the slip plane oriented at $-70.5°$ is nucleated during minimization. Thus an atomically sharp crack is even more unstable in orientation V than in orientation I.

So we switched to a blunt crack tip, again created by removing four planes of atoms. Simulations were performed using the same procedure as used for orientation I, except for the initial load level which is $K_I/\sqrt{r_1}\mu=0.19$. In all simulations the first event is the nucleation of a Shockley partial dislocation on the $(11\bar{1})$ slip plane. The load levels at which this happens are listed in Table III. The process is almost identical to that for orientation I: a row of roughly ten atoms crosses the barrier, after which the dislocation bows out with a speed of 2 nm ps$^{-1}$. The behavior is virtually independent of the potential type, the temperature, and the loading rate. The only difference from orientation I is that the nucleation occurs at a lower level of $K_I/\sqrt{r_1}\mu=0.37$.

### C. Orientation II

Unlike for orientations I and V, it is possible to create a stable atomically sharp crack for orientation II. However, this state is stable only over a small range of loading levels around $K_I/\sqrt{r_1}\mu=0.42$, for the LJ, Morse, as well as the EAM potentials. We have equilibrated conformations at this level and a range of temperatures for 4 ps using stochastic dynamics. The results of simulations at a range of temperatures and a range of relatively low loading rates are summarized in Table IV. At temperatures below 600 K the crack

TABLE III. The first events in the 44 simulations for a blunt crack tip in crystal orientations I and V. The numbers in the table are the strain values ($K_I/\sqrt{r_1}\mu$) at which the first event takes place, which is the nucleation of a Shockley partial dislocation on a slip plane oriented at angles of 35.3° and $-70.5°$ for orientations I and V, respectively.

| Orientation | Potential | No. of atoms | $T$ (K) | Loading rate $\dot{K}_I/\sqrt{r_1}\mu$ (ps$^{-1}$) $2.5\times10^{-2}$ | $1.0\times10^{-2}$ | $2.5\times10^{-3}$ | $10\times10^{-3}$ |
|---|---|---|---|---|---|---|---|
| I | LJ | 96 000 | 21 | 0.44 | 0.43 | 0.431 | 0.430 |
| I | LJ | 96 000 | 210 | 0.44 | 0.44 | 0.435 | 0.425 |
| I | Morse | 96 000 | 25 | 0.42 | 0.42 | 0.419 | 0.418 |
| I | Morse | 96 000 | 250 | 0.42 | 0.42 | 0.418 | 0.418 |
| I | Morse | 256 000 | 250 | 0.42 | 0.41 | 0.413 | 0.413 |
| I | EAM | 96 000 | 300 | 0.42 | | | 0.401 |
| V | LJ | 96 000 | 21 | 0.38 | 0.37 | 0.365 | 0.362 |
| V | LJ | 96 000 | 210 | 0.39 | 0.38 | 0.373 | 0.371 |
| V | Morse | 96 000 | 25 | 0.36 | 0.36 | 0.360 | 0.360 |
| V | Morse | 96 000 | 250 | 0.37 | 0.36 | 0.359 | 0.361 |
| V | EAM | 96 000 | 300 | 0.38 | | | 0.370 |

TABLE IV. Events at the crack tip for an atomically sharp crack in the 96 000-atom system in crystal orientation II. "c" indicates gradual crack propagation; "u" and "d" indicate dislocation nucleation on slip planes away from the crack tilted upward and downward, respectively, with the time (in picoseconds) at which the nucleation takes place.

| | $T$ | Loading rate $\dot{K}_I/\sqrt{r_1}\mu$ ($ps^{-1}$) | | | |
|---|---|---|---|---|---|
| Potential | (K) | $1.0\times10^{-3}$ | $2.5\times10^{-4}$ | $1.0\times10^{-4}$ | $2.5\times10^{-5}$ |
| LJ | 210 | | | c | |
| LJ | 420 | c | c | c | c |
| LJ | 630 | 41 d | 54 d | 33 u | |
| Morse | 500 | c | c | c | |
| Morse | 600 | | c | c | |
| Morse | 750 | 138 u | 96 u | 92 u | |
| Morse | 750 | | 92 d | | |
| EAM | 300 | c | c | | c |
| EAM | 600 | | c | | |

always propagates. The position of the crack tip is directly related to the strain level, independent of the strain rate. At temperatures above 600 K parts of both crack faces near the crack tip become disordered. This is also visible in the potential energy which shows a noisy decrease over the first nanosecond instead of a steady increase (not shown). During this disordering process a dislocation is nucleated from the crack tip. From the times shown in Table IV one can see that nucleation is not related to the value of $K_I$, as the times do not scale with the inverse of the loading rate. A probable explanation is that dislocations can only nucleate when a sufficient amount of disorder is present at the crack tip.

As for the other orientations, we have also performed simulations with a blunt crack tip that was created by removing four planes of atoms. To get a feeling for the statistical accuracy, an additional equilibration was performed for the LJ potential at 210 K, the Morse potential at 500 K, and the EAM potential at 10 K, using a different random seed for the initial velocities and for the stochastic dynamics. A total of 53 simulations at six loading rates between $\dot{K}_I/\sqrt{r_1}\mu = 1.0\times10^{-2}$ and $2.5\times10^{-5}$ $ps^{-1}$ have been carried out. Most simulations were started at a load level of $K_I/\sqrt{r_1}\mu = 0.38$, but those at the lowest two strain rates were started at $K_I/\sqrt{r_1}\mu = 0.42$. From the results given in Table V we can see that the crack always propagates with the LJ potential at 21 K and with the Morse potential at 250 K. Contrary to behavior with a sharp tip, the crack propagates rapidly over a significant distance, immediately invalidating the boundary conditions. At higher temperatures the first event is always the nucleation at the crack tip of a pair of forward Shockley partials on adjacent $(11\bar{1})$ slip planes. An example of the stress state just before nucleation is given in Fig. 4; a schematic picture of the geometry of the pair of partial dislocations is given in Fig. 5. In one Morse simulation and three EAM simulations two pairs of forward Shockley partial dislocations are nucleated simultaneously on $(11\bar{1})$ and $(1\bar{1}1)$ slip planes. At high loading rates crack propagation can occur simultaneously with the emission of the first dislocation. In all simulations the first pair of partial dislocations quickly expands in the $y$ direction and becomes periodic, before it moves away from the crack tip. This results in a stable situation where the dislocations have passed several rows of atoms enclosed between the two slip planes; an example of such a conformation is shown in Fig. 6. For the LJ and Morse potentials the number of rows is 3, 4, or 5; for the EAM potential 7, 8, or 9.

The load levels of the first events exhibit some consistent features. For the LJ and Morse potentials crack propagation at the lowest temperature always occurs at a lower strain level than dislocation nucleation at the intermediate temperature. For all three potentials the strain level for dislocation

TABLE V. The first events in the 53 simulations for a blunt crack tip at orientation II with $K_I$-continuum boundary conditions. The numbers in the table are the strain values ($K_I/\sqrt{r_1}\mu$) at which the first event takes place. "c" indicates crack propagation; "u" and "d" indicate dislocation nucleation on slip planes away from the crack tilted upward and downward, respectively.

| | | $T$ | Loading rate $\dot{K}_I/\sqrt{r_1}\mu$ ($ps^{-1}$) | | | | | |
|---|---|---|---|---|---|---|---|---|
| Potential | No. of atoms | (K) | $1.0\times10^{-2}$ | $2.5\times10^{-3}$ | $1.0\times10^{-3}$ | $2.5\times10^{-4}$ | $1.0\times10^{-4}$ | $2.5\times10^{-5}$ |
| LJ | 96 000 | 21 | 0.48 c | 0.475 c | 0.474 c | 0.471 c | 0.470 c | 0.469 c |
| LJ | 96 000 | 210 | 0.52 u+c | 0.491 u | 0.480 u | 0.478 u | 0.482 u | |
| LJ | 96 000 | 210 | 0.50 u+c | 0.489 u | 0.490 u | 0.480 u | 0.475 u | |
| LJ | 320 000 | 210 | 0.47 u | 0.485 u | 0.467 u | 0.473 u | 0.460 u | |
| LJ | 96 000 | 420 | 0.49 u | 0.482 u | 0.468 u | 0.467 u | | |
| Morse | 96 000 | 250 | 0.49 c | 0.481 c | 0.478 c | 0.476 c | 0.474 c | 0.472 c |
| Morse | 96 000 | 500 | 0.50 u | 0.482 u | 0.490 d+u | 0.480 u | | |
| Morse | 96 000 | 500 | 0.50 u | 0.487 u | 0.484 u | 0.470 u | | |
| EAM | 96 000 | 10 | 0.54 c | 0.522 c | 0.498 u | 0.489 u+d | | |
| EAM | 96 000 | 10 | 0.54 c | 0.521 u | 0.504 u | | | |
| EAM | 96 000 | 30 | 0.53 u+d | 0.511 u | 0.490 u | | | |
| EAM | 96 000 | 300 | 0.48 d+u | 0.481 u | 0.478 u | 0.477 u | | |

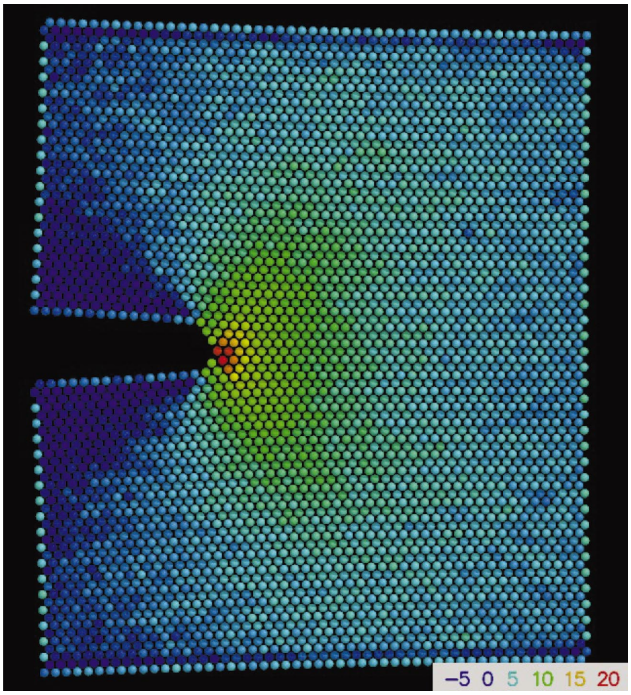


FIG. 4. (Color) The $\sigma_{zz}$ stress distribution (in GPa) for orientation II at $K_I/\sqrt{r_1\mu}=0.437$ for the 320 000-atom LJ system at a temperature of 210 K, with a loading rate of $\dot{K}_I/\sqrt{r_1\mu}=1.0\times10^{-3}$ ps$^{-1}$. The coordinates and the stress have been averaged over the 80 atoms along the crack front direction.

nucleation decreases with increasing temperature. Thus, the strain level at which dislocation nucleation occurs goes down as the temperature goes up, whereas the strain level for crack propagation increases with temperature. Both results are explained by the decrease of the elastic constants with increasing temperature. Lower elastic constants allow for more strain before bonds break, as well as shorter distances between atoms during dislocation nucleation.

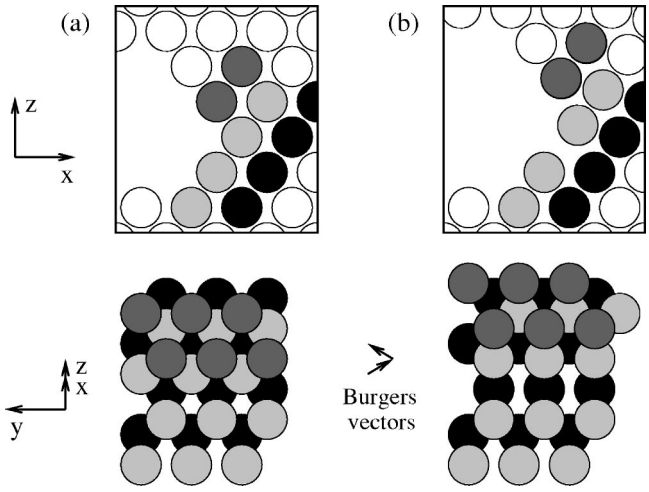


FIG. 5. Schematic drawing of the crack-tip region in orientation II before (a) and after (b) nucleation of two Shockley partial dislocations on adjacent slip planes. The two partials produce a net displacement between the two planes of dark-gray atoms which is in the *x*-*z* plane.

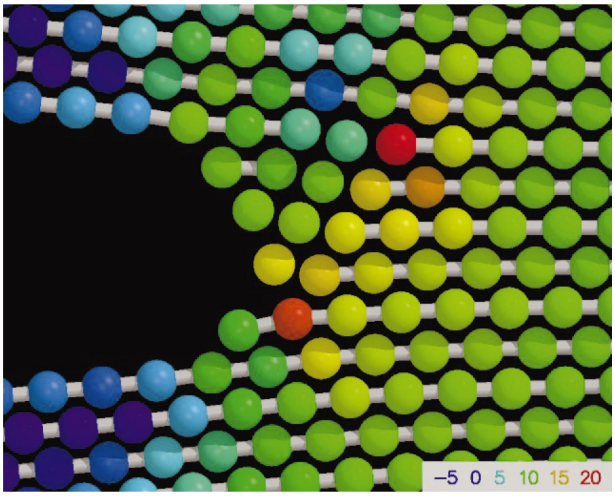


FIG. 6. (Color) The $\sigma_{zz}$ stress distribution (in GPa) for orientation II at $K_I/\sqrt{r_1\mu}=0.456$; that is, 20 ps later than in Fig. 4. Two Shockley partials have appeared on adjacent slip planes. The (100) crystal planes are marked with bond connections; the planes are interrupted by the dislocations. The four rows of atoms in between the slip planes are displaced by a half crystal spacing out of the picture.

In all LJ simulations at 210 K the second event is the nucleation of two forward Shockley partial dislocations at the position of the first two dislocations but on adjacent $(1\bar{1}1)$ slip planes. This happens between $K_I/\sqrt{r_1\mu}=0.52$ and 0.54. The pair of dislocations stops after it has moved along the slip planes over a distance of six rows of atoms. At this point the stress concentration has shifted from the crack tip to the last pair of dislocations; this invalidates the boundary conditions. With all three potentials at 300 K or above the same process occurs in most simulations, but between $K_I/\sqrt{r_1\mu}=0.55$ and 0.58, it is accompanied by movement of the first pair of dislocations to a total of 7–10 rows. In four of the simulations with the Morse potential the second pair of dislocations does not appear. In half of the simulations with the EAM potential the second event is the nucleation of a backward Shockley partial dislocation on an $(1\bar{1}1)$ slip plane.

We now look in more detail at the process of the nucleation of the first pair of partial dislocations. The mechanism is the same in all simulations. First one Shockley partial is nucleated, usually on the lower slip plane, and the dislocation on the adjacent slip plane follows almost immediately. A time sequence of the nucleation on the lower slip plane is shown in Fig. 7. Some not completely concerted motion can be observed in Fig. 7(a) for a row of about 20 atoms along the crack front. The transition state has been reached in Fig. 7(b), where 12 atoms in a row cross the barrier almost simultaneously. In Fig. 7(c) some atoms of the next row also cross the barrier. After that the dislocation rapidly expands sideways, i.e., in the *y* direction. Since the first pair of dislocations always involves the same two adjacent slip planes, we can easily look for fluctuations before the first event that did not develop into dislocations. We searched for atoms that were close to the barrier for nucleation of a Shockley partial

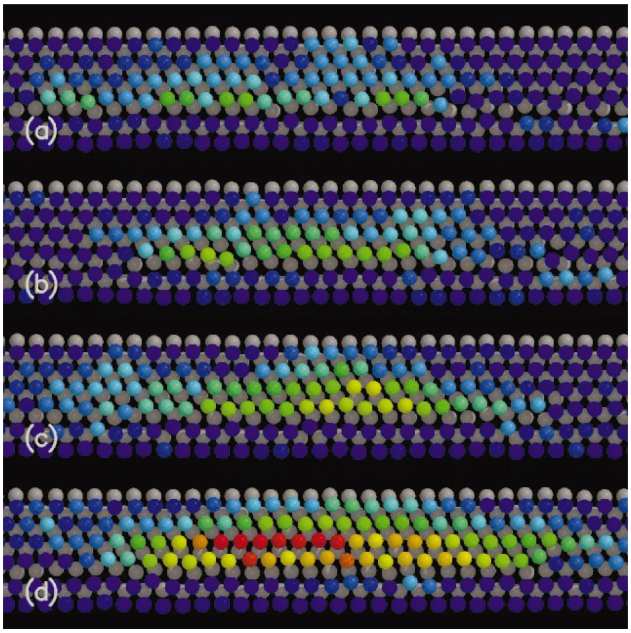


FIG. 7. (Color) Four snapshots of the system described in Fig. 4, at times 6.6 (a), 7.0 (b), 7.4 (c) and 7.8 ps (d) later in the simulation. The snapshots are taken perpendicular to the $(11\bar{1})$ slip plane of the nucleating Shockley partial dislocation. The crack front is located between the fourth and the fifth horizontal rows of blue atoms. Due to the dislocation the colored atoms move up and to the right with respect to the layer below (gray atoms) and the layer above (not shown). The atoms are colored according to their displacement in the horizontal direction; blue is the original position, green is at the transition state, and red is the final state after the partial dislocation has passed.

dislocation on each slip plane. We counted a fluctuation when at least two atoms had traveled 40% or more of the Burgers vector of the partial dislocation. In the LJ simulations at 210 K fluctuations start appearing at approximately $K_I/\sqrt{r_1\mu}=0.442$. We observed three fluctuations in simulations with $\dot{K}_I/\sqrt{r_1\mu}=2.5\times10^{-4}$ ps$^{-1}$, and eight and zero for $\dot{K}_I/\sqrt{r_1\mu}=10^{-4}$ ps$^{-1}$. The fluctuations have an average spacing in time of 8 ps; this is calculated using the time from the first fluctuation till the nucleation of the first dislocation. The average size is three atoms. At higher strain rates no fluctuations were observed. In the Morse simulations at 250 K a total of four fluctuations is observed before crack propagation occurs; this is not enough to determine a strain rate dependence. With the 320 000 system the number of fluctuations at $\dot{K}_I/\sqrt{r_1\mu}=2.5\times10^{-4}$ ps$^{-1}$ doubles to 6. In each of the simulations at the two higher strain rates two fluctuations are observed, and the time interval is halved to 4 ps. This is exactly the behavior one would expect: when the length of the crack front is doubled the probability of the occurrence of fluctuations also doubles. At $\dot{K}_I/\sqrt{r_1\mu}=10^{-4}$ ps$^{-1}$ the dislocations nucleate so early that only three fluctuations can be observed. In the simulations at 420 and 500 K, both potentials give rise to fluctuations already around $K_I/\sqrt{r_1\mu}=0.40$, at an average interval of 3 ps. There are seven fluctuations in all three simulations at $\dot{K}_I/\sqrt{r_1\mu}=2.5\times10^{-3}$ ps$^{-1}$ and roughly 70 at $\dot{K}_I/\sqrt{r_1\mu}=2.5\times10^{-4}$ ps$^{-1}$. The size of most fluctuations is around three atoms; the maximum size, which is observed several times, is 6 and 11 atoms for 210–250 and 420–500 K, respectively. Note that these numbers are not very accurate as they are dependent on the definition of a fluctuation as well as on the time resolution of the trajectories used for the analysis. The ratios between the different simulations, however, is likely to be correct.

Analysis of the fluctuations aids in explaining the behavior for orientation II. Because the Burgers vector for the Shockley partial dislocation as well as the path over the barrier point 60° out of the *x*-*z* plane, the stresses in the system do not pull the atoms in the correct direction for dislocation nucleation. Thermal fluctuations are required in which a small row of atoms moves mainly in the *y* direction. Such fluctuations can occur only when the crack tip is strained significantly. When the loading rate is very high there is not enough time for fluctuations to develop and the crack will propagate. At low loading rates, fluctuations occur and one of these could develop into a dislocation when the conditions are right. The probability for a fluctuation to occur is proportional to the length of the crack front and should be strongly dependent on the temperature. This is consistent with the observed number of fluctuations and the results given in Table V. It should be noted, though, that the fluctuations alone are not enough: in some simulations, as many as 70 fluctuations occur before a dislocation appears. This emphasizes that the strain at the crack tip needs to be high enough before the fluctuations can overcome the barrier to nucleate a dislocation.

## V. CONCLUSIONS

The competition between crack propagation and dislocation nucleation is quite sensitive to the type and rate of loading. In the shock-wave simulations, where we used planar-extension boundary conditions, dislocations appear independently of the temperature, the potential, and the applied extension rates. When the shock wave reaches the crack, the crack-tip region becomes disordered and dislocations are emitted, even at low temperatures. The disorder lowers the stress at the crack tip to such an extent that crack propagation becomes essentially impossible. In the regime with quasistatic $K_I$ boundary conditions, more subtle effects come into play. In crystal orientations I and V, dislocations are emitted under all conditions, whereas for orientation II crack propagation occurs for an atomically sharp crack, and for a blunt crack tip at low temperatures or high strain rates.

The crystal orientation is the most important factor in the competition between crack propagation and dislocation nucleation. Stress at the crack tip can be released by emitting dislocations in forward directions at an angle with the crack plane. In all three studied crystal orientations, {111} slip planes are available at such angles. However, the directions of the Burgers vector of the first Shockley partial dislocation differ significantly. In orientations I and V the Burgers vector is in the *x*-*z* plane. Therefore dislocations nucleate when the strain is so high that the row at the center of the crack tip is lifted over the row of atoms on the other side of the slip

plane. This has always been found to happen before crack propagation can occur. In orientation II the Burgers vector of the first Shockley partial dislocation makes an angle of 60° with the *x*-*z* plane. In this case, dislocation nucleation requires a sideways motion, which is not driven by the stresses in the system. The sideways motion needs to come from random thermal fluctuations which are temperature dependent. This explains why dislocations are observed only at higher temperatures. At lower temperatures no significant fluctuations occur and no dislocations are emitted. Thus the stresses at the crack tip rise until the crack propagates. Contrary to orientations I and V the first nucleation event in orientation II involves a pair of Shockley partial dislocations on adjacent slip planes. The length along the crack front of the nucleating dislocations is always around 12 atoms. It should be noted that for orientation II a quasi-2D simulation would underestimate the stress level at which the first dislocation is nucleated, as the sideways motion of a single atom along the crack front is not hindered by neighboring atoms present in the full 3D case.

The dislocation mechanism observed in orientation II requires thermal fluctuations to localize and thereby nucleate partial dislocations. Rice and Beltz[3] have carried out a continuum analysis of this process, which involves solving for a slip displacement field that can precipitate into a dislocation loop. The shape of their incipient loop is quite similar to what we predict in Fig. 7(d). The incipient slip field in their Fig. 8,[3] however, is more localized than what our atomistic results give.

We have not observed significant qualitative differences in the behavior with the LJ, Morse and EAM potentials. For crystal orientations I and V even the quantitative differences are negligible, which suggests that the behavior is determined only by the fcc crystal conformation. The only quantitative differences occur in crystal orientation II. In the shock-wave simulations with the LJ potential more dislocations are emitted than with the Morse potential. In the simulations with quasistatic $K_I$ boundary conditions the transition from crack propagation to dislocation emission happens at a lower temperature for the LJ potential than for the Morse potential and for the EAM potential dislocations can even nucleate at 10 K. In this orientation fluctuations of a single line of atoms along the crack front play an important role. Such fluctuations are energetically more favorable with the more shallow, long-ranged LJ potential than with the Morse potential. Due to the sublinear dependence of the EAM potential on the number of neighbors, the displacement of one row of atoms costs less energy than for the pair potentials. We would like to emphasize that insufficient equilibration, an incorrect treatment of cutoff effects, or a small error in the anisotropic continuum solution can have drastic effects on the results.

We conclude that at the atomic scale the crystal orientation is the most important factor in the competition between crack growth and dislocation emission. Only when the Burgers vector of partial dislocations is not aligned with the maximum resolved shear stress is this competition sensitive to temperature and type of potential. We expect that this applies not only when the crack front follows a ⟨011⟩ direction, as studied here, but in any direction.

Finally, we should point out that the competition between crack growth and dislocation emission in a single crystal is not necessarily decisive in the brittle-to-ductile transition of materials.[21] First of all, dislocation emission is not always a necessary condition, for instance because of the presence of preexisting dislocations, which are unavoidable in metals. On the other hand, emission is not a sufficient condition, because the dislocation may be hindered, for example, by lattice friction or other dislocations, to move away from the crack tip in order to shield it.

## ACKNOWLEDGMENTS

This work is part of the research program of the Foundation for Fundamental Research on Matter (FOM) and was financially supported by the Netherlands Organization for Scientific Research (NWO).

## APPENDIX

Sih and Leibowitz found the solution for the dominant term of the stress field around a crack tip in an anisotropic elastic medium under mode I loading.[19] Here we report the stress fields for the geometry where the crack extends along the negative $x$ axis in the $x$-$y$ plane, as in Fig. 1(b):

$$\sigma_{xx} = \frac{K_I}{\sqrt{2\pi r}}\mathrm{Re}\left[\frac{\mu_1\mu_2}{\mu_1-\mu_2}\left(\frac{\mu_2}{\sqrt{\cos\theta+\mu_2\sin\theta}} - \frac{\mu_1}{\sqrt{\cos\theta+\mu_1\sin\theta}}\right)\right],$$

$$\sigma_{zz} = \frac{K_I}{\sqrt{2\pi r}}\mathrm{Re}\left[\frac{1}{\mu_1-\mu_2}\left(\frac{\mu_1}{\sqrt{\cos\theta+\mu_2\sin\theta}} - \frac{\mu_2}{\sqrt{\cos\theta+\mu_1\sin\theta}}\right)\right],$$

$$\sigma_{xz} = \frac{K_I}{\sqrt{2\pi r}}\mathrm{Re}\left[\frac{\mu_1\mu_2}{\mu_1-\mu_2}\left(\frac{1}{\sqrt{\cos\theta+\mu_1\sin\theta}} - \frac{1}{\sqrt{\cos\theta+\mu_2\sin\theta}}\right)\right],$$

where $x=r\cos\theta$, $z=r\sin\theta$, and $\mu_1$ and $\mu_2$ are the complex roots of the characteristic equation

$$S'_{11}\mu^4 - 2S'_{16}\mu^3 + (2S'_{12}+S'_{66})\mu^2 - 2S'_{26}\mu + S'_{22} = 0.$$

The reduced elastic constants $S'_{ij}$ in Voigt notation are derived from the compliance matrix $S_{ij}$ as follows:

$$S'_{ij} = S_{ij} - \frac{S_{i3}S_{j3}}{S_{33}}.$$

The displacements are given by

$$u_x = K_I\sqrt{\frac{r}{\pi}}\mathrm{Re}\left[\frac{1}{\mu_1-\mu_2}[-\mu_2(\mu_1^2 S'_{11}-\mu_1 S'_{16}+S'_{12})\sqrt{\cos\theta+\mu_1\sin\theta}+\mu_1(\mu_2^2 S'_{11}-\mu_2 S'_{16}+S'_{12})\sqrt{\cos\theta+\mu_2\sin\theta}]\right],$$

$$u_z = K_I\sqrt{\frac{r}{\pi}}\mathrm{Re}\left\{\frac{1}{\mu_1-\mu_2}\left[-\mu_2\left(\frac{1}{\mu_1}S'_{22}-S'_{26}+\mu_1 S'_{12}\right)\sqrt{\cos\theta+\mu_1\sin\theta}+\mu_1\left(\frac{1}{\mu_2}S'_{22}-S'_{26}+\mu_2 S'_{12}\right)\sqrt{\cos\theta+\mu_2\sin\theta}\right]\right\}.$$


[1] J. R. Rice, J. Mech. Phys. Solids **40**, 239 (1992).
[2] G. E. Beltz and J. R. Rice, Acta Metall. Mater. **40** (Suppl.), S321 (1992).
[3] J. R. Rice and G. E. Beltz, J. Mech. Phys. Solids **42**, 239 (1992).
[4] G. Schöck, J. Mech. Phys. Solids **44**, 413 (1995).
[5] G. Xu, A. S. Argon, and M. Ortiz, Philos. Mag. A **72**, 415 (1995).
[6] G. Xu, A. S. Argon, and M. Ortiz, Philos. Mag. A **75**, 341 (1997).
[7] S. J. Zhou, D. M. Beazley, P. S. Lomdahl, and B. L. Holian, Phys. Rev. Lett. **78**, 479 (1997).
[8] F. F. Abraham, R. Walkup, H. Gao, M. Duchaineau, T. Diaz de la Rubia, and M. Seager, Proc. Natl. Acad. Sci. U.S.A. **99**, 5783 (2002).
[9] P. C. Gehlen, G. T. Hahn, and M. F. Kanninen, Scr. Metall. **6**, 1087 (1972).
[10] P. C. Gehlen, Scr. Metall. **7**, 1115 (1973).
[11] P. Gumbsch, J. Mater. Res. **10**, 2897 (1995).
[12] R. Miller, E. B. Tadmor, R. Phillips, and M. Ortiz, Modell. Simul. Mater. Sci. Eng. **6**, 607 (1998).
[13] J. A. Zimmerman, H. Gao, and F. F. Abraham, Modell. Simul. Mater. Sci. Eng. **8**, 103 (2000).
[14] H. J. C. Berendsen, D. van der Spoel, and R. van Drunen, Comput. Phys. Commun. **91**, 43 (1995).
[15] E. Lindahl, B. Hess, and D. van der Spoel, J. Mol. Model. [Electronic Publication] **7**, 306 (2001).
[16] D. Oh and R. Johnson, in *Atomistic Simulation of Materials: Beyond Pair Potentials*, edited by V. Vitek and D. Srolovitz (Plenum Press, New York, 1989), pp. 233–238.
[17] H. J. C. Berendsen, J. P. M. Postma, W. F. van Gunsteren, A. DiNola, and J. R. Haak, J. Chem. Phys. **81**, 3684 (1984).
[18] G. A. Alers, J. R. Neighbours, and H. Sato, J. Phys. Chem. Solids **13**, 40 (1960).
[19] G. C. Sih and H. Leibowitz, *Fracture* (Academic Press, New York, 1968), Vol. 2, Chap. 2, pp. 67-190.
[20] W. C. Crone, T. W. Shield, A. Creuziger, and B. Henneman, J. Mech. Phys. Solids **52**, 85 (2004).
[21] P. Gumbsch, J. Riedle, A. Hartmaier, and H. F. Fischmeister, Science **282**, 1293 (1998).